INTERNATIONAL JOURNAL OF
COASTAL, OFFSHORE & ENVIRONMENTAL ENGINEERING IJCOE Vol.8/No. 4/8XWXPQ 2023 (9-17)

Available online at: www. Ijcoe.org

Sensitivity Analysis of Makran Subduction Zone's Seismic Parameters for Optimizing the Number of Potential Tsunami Scenarios

Ehsan Rastgoftar[1*], Ali Khoshkholgh[1], Mahmood Reza Akbarpour Jannat[1]

[1] Iranian National Institute for Oceanography and Atmospheric Science, Tehran, Iran,
Corresponding author:e.rastgoftar@inio.ac.ir

ARTICLE INFO

Article History:
Received: 06 Sep. 2023
Accepted: 19 Sep. 2023

Keywords:
Tsunami
Makran Subduction Zone
Earthquake Magnitude
Dip Angle
Rake angle

ABSTRACT

Given the necessity of knowing the probability and risk of future tsunamis in actions related to tsunami hazard mitigation, the Probabilistic Tsunami Hazard analysis (PTHA) approach has been accepted as the basis for tsunami risk assessment studies for high-risk areas such as the Makran region. Considering the uncertainties associated with fault parameters and the random nature of earthquake occurrence in PTHA, simulation a large number of potential tsunami scenarios is required in future tsunami studies of the Makran Subduction Zone (MSZ). In order to optimize the number of scenarios in these studies, appropriate values for the ranges and change intervals of some uncertain seismic parameters in different scenarios are determined in the present study. For this, the values used in previous studies for earthquake magnitude and depth as well as dip and rake angles of MSZ's tsunamigenic earthquakes are investigated; and the effects of variations in these parameters on the tsunami waves are evaluated through numerical modeling based on non-linear shallow water equations and sensitivity analysis.

The obtained results show that a minimum value of Mw0.1 for the interval of earthquake magnitude variations must set in developing potential tsunami scenarios for the Makran region. Also, considering two or three values in the range of 2º to 20º and 10 km to 30 km, respectively, as probable values for the dip angle of the subduction zone and the depth of tsunamigenic earthquakes seems sufficient. However, if the minimum number of scenarios is desired, selecting a unit value for the dip angle in the range of 10º to 15º and a constant earthquake depth of 10 km can be acceptable. Also, for rake angle a constant value of 90º can be considered in different scenarios.

1. Introduction

Tsunamis, despite their infrequent occurrence, are considered one of the greatest threats to human communities. According to available statistics, the 2004 Indian Ocean tsunami, with over 220,000 human casualties, remains the deadliest natural disaster of the present century by a large margin. The list also includes the 2011 Tohoku tsunami and 2018 Sulawesi tsunami. The significant loss of life and property damage associated with tsunamis makes them a high-risk event, despite their low probability. Therefore, understanding and assessing tsunamis and preparing for them is of utmost importance and special attention in coastal areas at risk.

Although any factor that suddenly displaces a large volume of seawater falls among the sources of tsunami (like landslide, volcanic activity …), the earthquakes resulted from the subduction of tectonic plates are recognized as the most common cause of tsunamis. According to "Global Historical Tsunami Database" [1] from 1900 to the present, more than 80% of potential tsunamis have been triggered by earthquakes. Among the earth's subduction zones, the Makran Subduction Zone (MSZ) is known as s susceptible region for generating tsunamis in the Indian Ocean (along with the Sunda subduction zone). Formed as a result of the collision of the Arabian plate with the Eurasian plate, this zone extends approximately 900 kilometers along the northwest of the Indian Ocean, adjacent to the southern coasts of Iran and Pakistan. The available evidences suggest fewer huge earthquakes in the Makran region compared to other subduction zones; however several significant earthquakes and tsunami events have been reported in this area. The most notable of these is the earthquake

and accompanying tsunami in 1945, which caused the death of over 4,000 people totally [2].

Before 2004, the occurrence of tsunamis in the Sunda subduction zone (at least its northern part) was considered unexpected, mostly because of the lack of historical data related to large earthquakes during the past 200 years. Following the occurrence of the massive earthquake and tsunami in 2004, more detailed studies revealed evidence of large tsunamis in the 1000-year-old sediment layers [3]. A similar situation could be true for the Makran region, especially in relation with its western part, which has showed lower seismic activity compared to the eastern part and has not experienced a major earthquake in recent centuries (at least in the past 600 years) [4].

Numerous studies have been conducted regarding the assessment of tsunamis in the Makran region. These studies initially focused on the modeling of the 1945 tsunami (or similar tsunamis) [5, 6, 7, 8, 9, and 10]. Subsequently, another category of studies formed, based on a deterministic analysis approach, in which limited and specific scenarios of potential earthquakes and tsunamis (mostly worst-case scenarios) were simulated [11, 12, and 13]. In recent years, a new series of studies has emerged to determine the probability of tsunami intensity, using a probabilistic tsunami hazard analysis (PTHA) approach [3, 14 and 15]. In these studies, by estimating earthquake occurrence rates, all possible tsunami scenarios, ranging from small to large events, along with all estimable uncertainties, are considered to assess tsunami risk.

Considering the need for probabilistic assessment and risk estimation of future tsunamis in decision-making processes related to tsunami hazard mitigation [16], PTHA studies for tsunami-prone regions is essential. For example, according to the American loading standard (ASCE/SEI 7-16), which can be considered the most comprehensive reference for considering the effects of tsunamis in structural design, the "design tsunami" is defined as an event with a 2% probability of being exceeded in a 50-year period and it should be determined based on a site-specific probabilistic tsunami hazard analysis approach [17].

In the PTHA approach all tsunami sources and uncertainties associated with tsunamis are usually considered through the implementation of a logic tree approach. The existing uncertainties, containing epistemic uncertainties related to fault parameters and aleatory uncertainties related to the random nature of earthquake occurrence and the inability to predict their magnitude and location, lead to the creation of various nodes in the developed logical tree. As a result, the PTHA approach involves simulating a large number of defined scenarios, the number of which reaches thousands depending on the diversity of uncertain parameters and the intervals for their values.

It should be noted that the necessity of simulating a large number of possible tsunami scenarios in the Makran region does not only include PTHA-related studies. Since the MSZ is located on the margins of the Indian Ocean at a very short distance from the coasts, it is a nearfield tsunami source for many neighboring countries such as Iran, Pakistan, Oman, and India. Its possible earthquakes can occur in close proximity to coastal areas or even inland. This means that the resulting tsunamis will reach the coasts of neighboring countries within a very short time interval (between 20 minutes to 1 hour), which makes the tsunami warning process very difficult. Therefore post-event tsunami simulation is not feasible for tsunami warning centers, and it is essential to have comprehensive databases extracted from pre-simulated probable tsunami scenarios available at these centers.

It is obvious that simulating a very large number of tsunami scenarios is computationally and time-intensive and is not desirable. What causes the multiplicity of these scenarios is the variations in the uncertain values of fault parameters and the random information related to the magnitude and location of earthquakes in different scenarios. In order to prevent unnecessary growth in the number of scenarios, the mentioned parameters variations should occur within the range of real and logical values. Furthermore, the steps of changes should be optimally selected in a way that excessive small steps do not cause the number of scenarios to increase unnecessarily. At the same time, it is necessary to avoid applying large change intervals leading to missing scenarios with serious differences.

With the aim of preventing the simulation of an excessive number of tsunami scenarios in future studies of tsunami assessment in the MSZ, in the present study suitable values for the range and steps of changes for some seismic parameters in different scenarios are determined. For this purpose, firstly the proposed or applied values for earthquake magnitude and depth as well as dip and rake angles of MSZ's tsunamigenic earthquakes in previous studies are investigated. Then, the effects of variations in these parameters on the subsequent tsunamis are evaluated through numerical modeling and sensitivity analysis. In the numerical modeling, the initial tsunami wave is generated using Okada's rectangular elastic half-space model [18]; the wave propagation is calculated based on the nonlinear shallow water equations solved in a nested grid model domain centered on the Chabahar Bay area. Finally, the tsunami wave height in the vicinity of the bay is evaluated as a sensitivity parameter for simulation.

2. Uncertain Seismic Parameters

For the modeling of seismic tsunamis, the occurrence of the earthquake is usually considered instantaneous and the temporal changes of ground deformation are disregarded. Thus, the generated seabed displacement is identically transferred to the water free surface providing the initial tsunami wave. Among the several algorithms have been proposed to calculate the seabed

dislocation, the Okada's half-space elastic method [18] is used in the intended numerical model. In this method, the deformation of the seabed is calculated using analytical stress-strain relationships and earthquake source parameters including fault length, fault width, slip amount on the fault surface, dip angle, strike angle, rake angle, and focal depth. Among these parameters, the surface rupture length (L), down-dip rupture width (W), and slip amount on the fault surface (Δ) are directly dependent on the earthquake magnitude. The empirical relationship between seismic moment (M_0) and moment magnitude (M_w) (Eq.(1)), along with the seismic moment formula connecting the released energy of the earthquake to the product of the fault surface area, average slip in the fault zone, and the rigidity of the earth (Eq.(2)), indicates the dependency.

$$M_w = \frac{2}{3} log_{10}^{(M_0)} - 6 \quad (1)$$

$$M_0 = \mu \Delta L W \quad (2)$$

Despite the advancements in human knowledge, it is still not possible to accurately predict the magnitude and location of future earthquakes. Possible earthquakes can occur at any point along the fault or subduction zone with different magnitudes and dimensions. Therefore, within probable tsunami scenarios for each region earthquakes with different magnitudes are considered, and accordingly, the parameters of fault length, width, and slip also vary. The depth of earthquake is another uncertain seismic parameter, which cannot be predicted for future events and varies in the earthquake and tsunami scenarios. Other required seismic parameters, such as the dip, slip, and strike angles within a specific subduction zone, like the Makran region, change within a limited range. Although some studies on the structure and geology of MSZ have been started in recent years (e.g.[19]), the precise values of the dip and rake angles for the Makran region have not been completely clear, and different numbers have been reported for them in various sources. Therefore, based on previous studies, the magnitude and depth of MSZ's potential earthquakes, as well as possible values for the dip and rake angles, are investigated, and the appropriate values are obtained for sensitivity analysis of these parameters.

3.1. Earthquake Magnitude

The earthquake magnitude is the most important variable parameter in tsunami scenarios, as it affects other dependent parameters such as fault length, fault width, and slip amount on the fault surface. Subduction earthquakes with magnitudes less than Mw7.5 usually do not generate tsunamis [20]. Earthquakes smaller than this value (up to Mw6.5) may only cause slight changes in sea level near the epicenter. On the other hand, the largest probable earthquake in seismic regions is determined based on seismicity and tectonic characteristics. Different values have been reported as the largest probable earthquake in the MSZ. Employing the instrumental earthquake catalogues, due to their short time period, underestimates the maximum magnitude [15]. Based on the dependency of the largest expected earthquake on the length of the continuous fault system along the convergent plate boundary, a moment magnitude Mw 9.0 earthquake, corresponding to full rupture of the plate boundary, was considered as the largest tsunami source in the Makran region [11]. According to the MSZ's approximate length of 900 kilometers, the occurrence of earthquakes up to Mw8.8 was found also possible [21]. Moreover, thermal modeling results indicate the potential of MSZ for generating earthquakes ranging from Mw8.7 to Mw9.2 [22]. Therefore, to cover all potential tsunami-generating earthquakes (in terms of magnitude), in sensitivity analysis scenarios the magnitude of earthquake varies between Mw7 and Mw9 at intervals of 0.1. According to empirical relationships of Wells and Coppersmith [23], the length, width, and slip of a fault vary in proportion to the earthquake magnitude. However, considering the formula between seismic moment and moment magnitude (Eq.(1)) and the equation for seismic moment (Eq.(2)), the predicted values are slightly modified. Table 1 shows the changes in earthquake magnitude and its related parameters during the sensitivity analysis. It is obvious that other seismic parameters are assumed to be constant during this analysis (Table 2).

Table 1. Variation of earthquake magnitude and related parameters during sensitivity analysis

Moment magnitude	Fault length (km)	Fault width (km)	Fault slip (m)
Mw 7.0	40	20	1.11
Mw 7.1	50	20	1.25
Mw 7.2	60	20	1.47
Mw 7.3	70	20	1.79
Mw 7.4	80	20	2.21
Mw 7.5	90	20	2.77
Mw 7.6	110	30	2.14
Mw 7.7	120	30	2.76
Mw 7.8	150	30	3.12
Mw 7.9	170	30	3.89
Mw 8.0	200	40	3.51
Mw 8.1	230	40	4.31
Mw 8.2	270	40	5.18
Mw 8.3	320	40	6.18
Mw 8.4	380	50	5.88
Mw 8.5	440	50	7.17
Mw 8.6	520	60	7.14
Mw 8.7	600	60	8.74
Mw 8.8	710	60	10.44
Mw 8.9	830	70	10.81
Mw 9.0	980	70	12.93

Table 2. The values of fixed seismic parameters for sensitivity analysis

Sensitivity analysis seismic parameter	Fixed seismic parameters							
	Earthquake magnitude	Fault length	Fault width	Fault Slip	Dip angle	Rake angle	Earthquake depth	Strike angle
Earthquake magnitude	---	---	---	---	8º	90º	5 km	270º
Dip angle	Mw 8.7	600 km	60 km	8.74 m	---	90º	5 km	270º
Rake angle	Mw 8.7	600 km	60 km	8.74 m	8º	---	5 km	270º
Earthquake depth	Mw 8.7	600 km	60 km	8.74 m	8º	90º	---	270º

3.2. Dip Angle

Dip angle of a subduction zone, presenting the angle between the oceanic plate and the continental plate, describes the contact between the two tectonic plates according to the geometry of contact surface. With regards to increase in curvature of the contact area of the two plates with increasing depth, the dip angle of a subduction zone is not constant and usually grows with the depth of the earthquake. Due to the low level of seismic activity in the MSZ and limited data on past earthquakes, there is not accurate information regarding the dip angle and its variations with depth. In a study by Byrne et al. [24] on some earthquakes in the Makran region, the estimated dip angle values range from 7º to 27º (Table 3). According to the estimated value of 7º for the dip angle of the 1945 earthquake, many studies related to simulating the tsunami in the MSZ have used 7º as the dip angle [6, 9, 11, 25, and 26]. However, other values such as 10º [27] and 3º [28] have also been considered. Rashidi et al. [3] in modeling of Makran's potential tsunamis, set the dip angle range between 2º and 8º; maybe based on the results obtained from seismic reflection profiles along the MSZ indicating a relatively small dip angle between 2º and 8º [29]. With regard to the aforementioned points, for the sensitivity analysis of the dip angle the range of this parameter is considered to be 2º and 20º (in 3º degree intervals). The values of other seismic parameters are provided in Table 2.

Table 3. Seismic parameters of Makran earthquakes [24]

Date	Latitude (ºN)	Longitude (ºE)	Dip angle (º)	Rake angle (º)	depth (m)
Nov.27 1945	25.15	63.48	89	7	27
Aug.5 1947	25.04	63.49	68	7	20
Sept.1 1962	25.60	65.22	80	10	18
Feb.13 1969	24.99	62.75	84	9	18
Aug.6 1972	25.04	61.22	114	22	33
Aug.18 1972	24.83	63.14	84	9	20
Sept.2 1973	24.88	63.21	70	23	18
July 29 1975	25.22	63.09	88	27	18

3.3. Rake angle

The rake angle determines the movement of a fault relative to its strike, where values of 0º and 90º respectively represent strike-slip faulting and dip-slip faulting. Usually dip-slip faulting, by creating vertical displacement in the seafloor, leads to the formation of tsunami. A study of 36 earthquakes that generated tsunamis in different subduction zones shows that their average rake angle is approximately 91º [30]. However, full dip-slip faulting is rare in nature, and dip-slip faults often also have a component of strike-slip motion. According to Table 3, the estimated rake angle for dip-slip earthquakes in the MSZ varies between 68º and 114º. Considering the estimated value of 89º for the rake angle of the 1945 earthquake, simulations of the MSZ tsunami usually adopt a value of 89º or 90º for this seismic parameter. However, other values such as 100º have also been considered in some studies [31]. Therefore, for sensitivity analysis, the rake angle in simulations ranges from 70º to 120º (in 10º intervals).

3.4. Earthquake depth

The typical depth of earthquakes that generate tsunamis is less than 30 kilometers [31]. Earthquakes with greater source depths cannot effectively transfer energy to the seafloor and are unable to cause significant displacement of the ocean bed. The average depth of the 36 studied tsunamigenic earthquakes is estimated to be around 25 kilometers [30]. Table 3 indicates that the estimated depth of the earthquakes in the Makran region is less than 33 kilometers. Considering the depth of 27 kilometers for the 1945 earthquake, simulations of the MSZ tsunamis often assume a quake depth of 25 kilometers. Based on the above, the range of source depth variations for sensitivity analysis is considered to be values less than 35 kilometers (in 5-kilometer intervals).

3. Numerical Modeling

Like the usual approach of tsunami simulation, the variations in the free surface elevation obtained from tsunami generation phase (initial tsunami wave) are introduced as initial conditions to the tsunami propagation equations. Since the wavelengths of seismic tsunamis (hundreds of kilometers) are much larger than the ocean depth (a few kilometers), their propagation is usually calculated using shallow water equations, which are the simplest type of depth-averaged wave equations. In the MOST model [32],

used as the numerical model in this study, non-linear shallow water equations (NSW) are employed, which are expressed in Cartesian coordinates as follows:

$$\frac{\partial(\eta+d)}{\partial t}+\frac{\partial(u(\eta+d))}{\partial x}+\frac{\partial(v(\eta+d))}{\partial y}=0 \quad (3)$$

$$\frac{\partial u}{\partial t}+u\frac{\partial u}{\partial x}+v\frac{\partial u}{\partial y}+g\frac{\partial(\eta+d)}{\partial x}=g\frac{\partial d}{\partial x} \quad (4)$$

$$\frac{\partial v}{\partial t}+u\frac{\partial v}{\partial x}+v\frac{\partial v}{\partial y}+g\frac{\partial(\eta+d)}{\partial y}=g\frac{\partial d}{\partial y} \quad (5)$$

where η represents the free surface elevation (tsunami wave height), d is the still water depth, g is the gravitational acceleration, and u and v are the mean velocities at depth in the x and y directions, respectively. Considering that tsunami waves may travel long distances on the order of hundreds or thousands of kilometers before reaching coastal areas, for a more accurate representation of wave propagation over this long distance, factors such as seabed topography and the Coriolis force are also taken into account in the MOST model. Additionally, the effects of wave dispersion, which are not seen in the NSW equations, are approximately considered in the MOST model by utilizing the inherent numerical dispersion of the finite difference method.

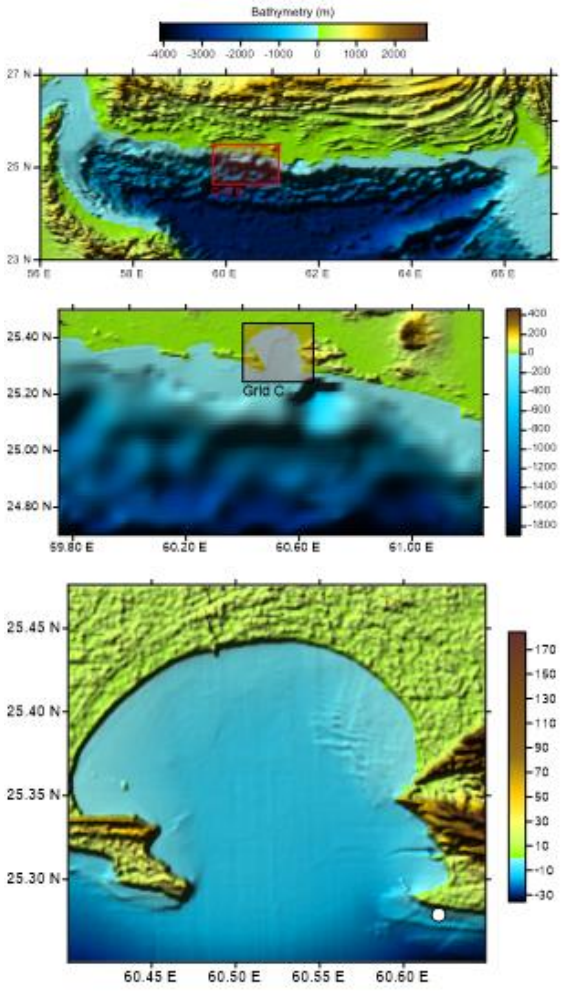

Figure 1. Values of hydrographic and topographic data of modeling grids; large-scale grid (top), intermediate grid (middle), coastal grid (bottom). The white circle indicates the position of the numerical wave station.

Due to the very long wavelengths of seismic tsunamis, considering computational points containing water depth information at distances apart (on the order of kilometers) may be sufficient for modeling tsunami generation and propagation in deep water. However, as the tsunami waves propagate towards the shore and the water depth decreases, the wavelength of the waves decrease. On the other hand, the impact of tsunami waves on coasts and the extent of run-up mainly depend on the complex effects of sea depth and coastal topography in the vicinity of the coastal region. Therefore, the governing equations for tsunami propagation (Eq.(3) to Eq.(5)) are solved here in a three-level nested grid model domain; moving from deep water toward the target coastal areas (Chabahar Bay) the grid resolution increases (Figure 1).

4. Results

In order to evaluate the results of sensitivity analysis, the wave height of the tsunami resulting from the simulations has been extracted at a point near Chabahar port (60.62º E - 25.28ºN) with a depth of approximately 50 meters (Figure 1). The recorded time series of waves during the sensitivity analysis of earthquake magnitude are shown in Figure 2 in two separate graphs (due to significant changes in tsunami wave height with earthquakes size). Also, Figure 3 shows the maximum recorded tsunami wave height for all earthquakes.

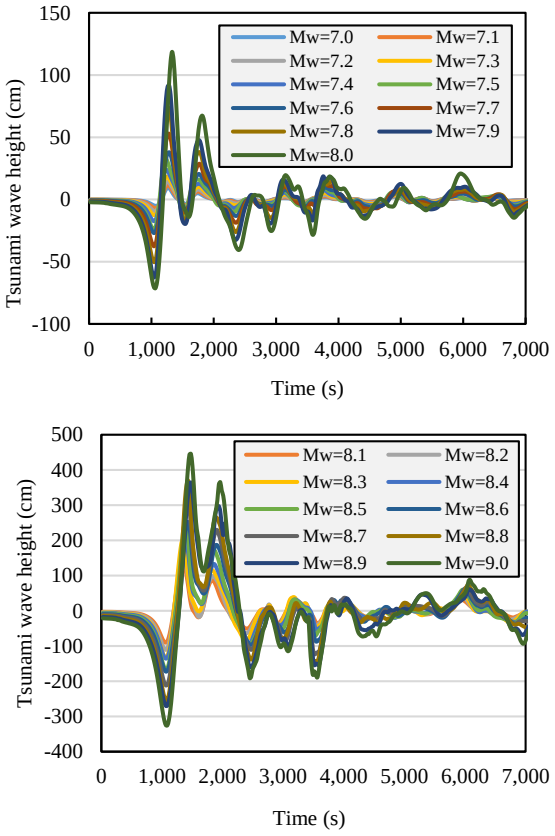

Figure 2. Time series of tsunami waves recorded during the sensitivity analysis of earthquake magnitude.

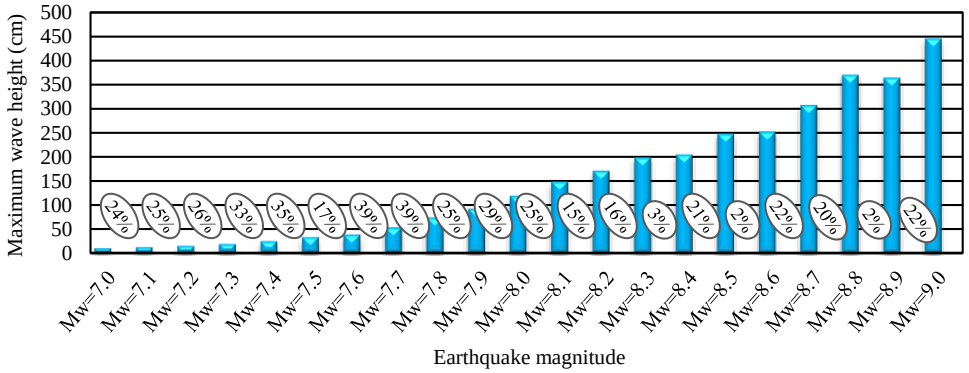

Figure 3. variation of maximum tsunami wave height with earthquake magnitude.
The numbers inside the circles indicate the amount of change in wave height between successive intervals of earthquake magnitude.

It is observed that, as expected, the height of the tsunami wave increases with the magnitude of the earthquake. However, as can be seen in Figures 2 and 3, this trend is violated in some cases, and the height of the waves does not always increase with the increase in earthquake magnitude.

By carefully examining Table 1, it can be realized that the main cause of this is mainly related to variations in the amount of slip in the scenarios. For example, between Mw8.5 to Mw8.6 and also Mw8.8 to 8.9 earthquake scenarios, the amount of slip does not increase significantly, and as a result, the calculated wave height does not rise significantly either. The source of this non-uniform trend is related to the way of determining the amount of slip in the scenarios; here, for each scenario, firstly the length and width of the fault was estimated according to the earthquake magnitude and the applied empirical relationships, and then the amount of slip was determined in such a way that the relationship between magnitude and earthquake moment (Eq.(1)) is satisfied. This has caused the amount of slip, which is a key parameter determining the height of tsunami waves, to not change proportionally with the earthquake magnitude in sensitivity analysis scenarios (Table 1). Another point is related to the pattern of tsunami wave propagation near the coast; due to the variation in fault size in different scenarios, the pattern of tsunami wave propagation also changes, which leads to wave reflection and amplification, and can cause larger waves for smaller earthquake scenarios.

The time series in Figure 4, corresponding to the sensitivity analysis of dip angle, demonstrate that with an increase in the of dip angle, the ocean floor uplift and subsequently the tsunami wave height increase. However, the tsunami height changes due to dip angle variation are not significant, as shown in Figure 5 (the numbers inside the circles). The maximum tsunami wave height varies by approximately 10% for successive scenarios with a 3º change in dip angle.

The variations of tsunami wave height with changes in the rake angle are shown in Figures 6 and 7. Based on the obtained results, the changes in tsunami height due to changes in the rake angle are very small (about 5%).

Additionally, as expected, the maximum tsunami wave height is observed during the rake angle of 90 degrees (full dip-slip faulting).

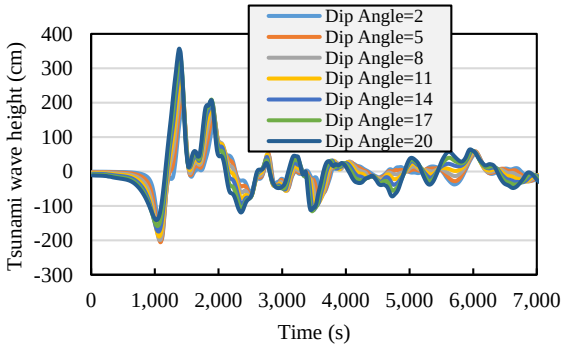

Figure 4. Time series of tsunami waves recorded during the sensitivity analysis of dip angle.

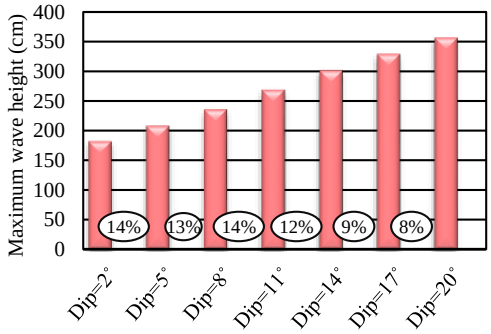

Figure 5. Variation of maximum tsunami wave height with dip angle. The numbers inside the circles indicate the amount of change in wave height between successive intervals of dip angle.

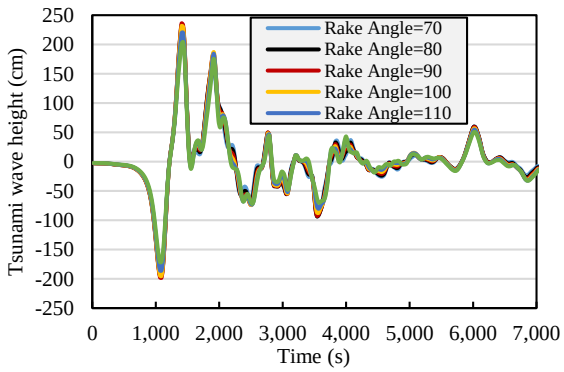

Figure 6. Time series of tsunami waves recorded during the sensitivity analysis of rake angle.

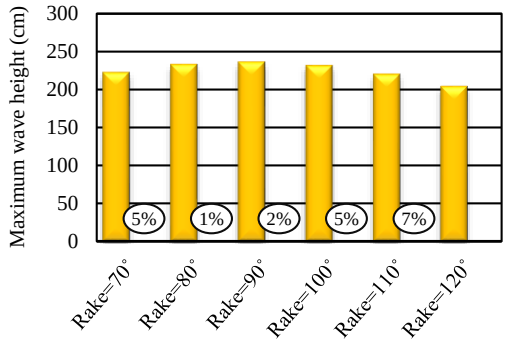

Figure 7. Variation of maximum tsunami wave height with rake angle. The numbers inside the circles indicate the amount of change in wave height between successive intervals of rake angle.

The simulation results related to the sensitivity analysis of the depth of the earthquake (Figures 8 and 9) indicate that although, as expected, with an increase in the focal depth, the displacement of the ground surface and subsequently the tsunami wave height decrease, but this trend is not accurate in the first step, meaning that a of 5-kilometer earthquake depth has resulted in smaller waves in comparison to a similar earthquake at a depth of 10 kilometers.

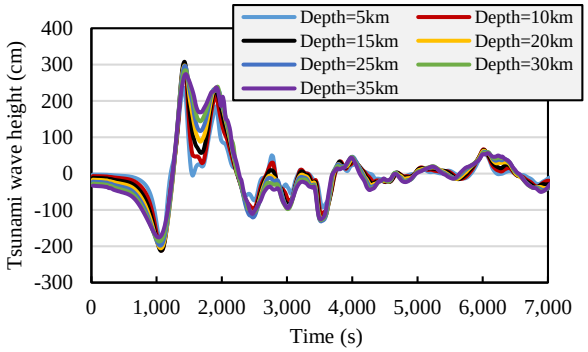

Figure 8. Time series of tsunami waves recorded during the sensitivity analysis of earthquake depth.

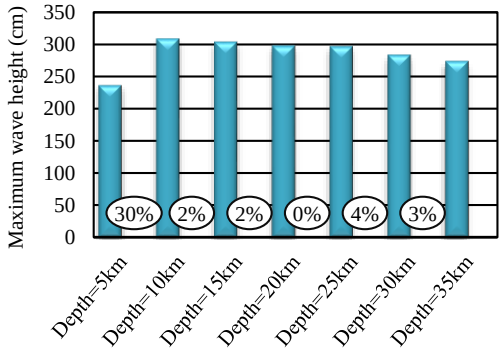

Figure 9. Variation of maximum tsunami wave height with earthquake depth. The numbers inside the circles indicate the amount of change in wave height between successive intervals of earthquake depth.

In order to be more sure about the accuracy of the results of the of earthquake depth sensitivity analysis, in addition to the nearshore wave station, the tsunami wave height has also been recorded at another point in the deep water area of Chabahar Port (at a depth of 1600 meters) (Figures 10 and 11). Again, it is observed that an earthquake depth of 10 kilometers creates the highest wave height. Furthermore, the changes in tsunami height due to a 5-kilometer change in earthquake depth are relatively small (less than 10 percent). the comparison of the recorded waves at the two numerical stations also shows that the nearshore waves (with a height of 2.5 to 3 meters) are higher than the deep water waves (with a height of 1 to 1.5 meters).This can be attributed to the increase in the height tsunami waves as they approaches the coast due to shoaling.

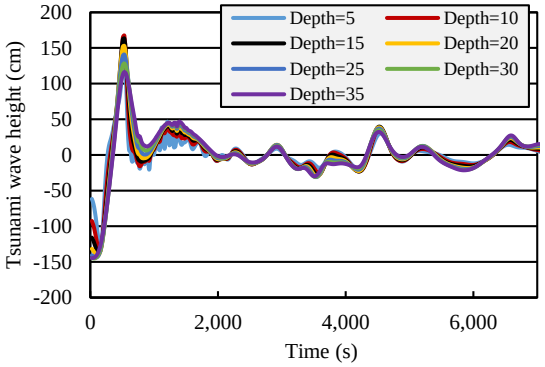

Figure 10. Time series of tsunami waves recorded during the sensitivity analysis of earthquake depth (at the deep water numerical wave station).

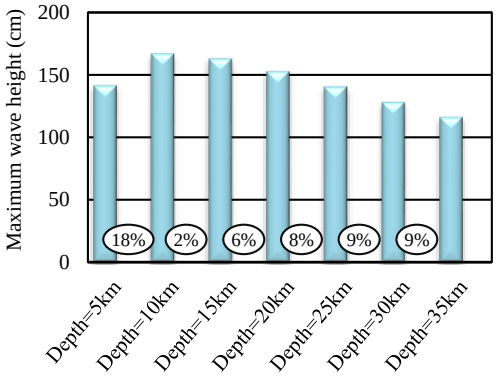

Figure 11. Variation of maximum tsunami wave height with earthquake depth. The numbers inside the circles indicate the amount of change in wave height between successive intervals of earthquake depth (at the deep water numerical wave station).

5. Conclusion

The review of studies on MSZ's tsunami hazard assessment showed that PTHA is currently recognized as an essential approach for conducting these studies. Therefore, due to taking into consideration all of the uncertainties associated with tsunamis in PTHA, the simulation of a large number of possible tsunami scenarios will be inevitable for future MSZ's tsunami studies, which requires high computational costs. The number of these scenarios are a function of the diversity of included uncertain seismic parameters and the

considered intervals for their values. In order to reduce and optimize the number of scenarios in future studies of tsunami assessment in the Makran region, the proposed values of some MSZ's uncertain seismic parameters, including earthquake magnitude and depth as well as dip and rake angles, in previous studies were investigated. After that, using numerical modeling and sensitivity analysis, the effects of variations in the mentioned parameters on the subsequent tsunamis were evaluated. Finally, based on the obtained results, the range and change interval of these seismic parameters are suggested as following:

Earthquake magnitude: Since change in earthquake magnitude in intervals of Mw 0.1 considerably affect the tsunami waves, with an average change of approximately 20% in wave height at each step (Figure 2 and 3), use of a value of Mw 0.1 as the minimum interval of earthquake magnitude variations seems necessary for comprehensive tsunami scenarios in the Makran region. However, considering that tsunamis caused by earthquakes smaller than Mw 8 are less hazardous and have wave heights less than 1 meter (Figure 3), in order to reduce the number of simulation scenarios, it is possible to set slightly larger steps for magnitude variations in this range (Mw <8).

Dip angle: according to the slight changes in tsunami height caused by 3-degree variations in dip angle (Figure 4), considering two or three values in the range of 2º to 20º degrees as possible values for the dip angle seems sufficient for developing MSZ's tsunami scenarios. However, if the minimum number of scenarios is desired, due to the direct relationship between dip angle and tsunami height (Figure 5), a constant value in the range of 10 to 15 degrees can be set for the this angle (with a little overestimation of tsunami waves).

Rake angle: Due to the very slight changes in waves of tsunami height corresponding to variations in rake angle (Figures 6 and 7), it is not necessary to change the rake angle values when possible tsunami scenarios of MSZ is defined. Considering a constant value of 90 degrees for the slope angle, as the value leading to maximum tsunami wave height (Figure 7), in different scenarios seems reasonable.

Earthquake depth: since the 5-kilometer variations in earthquake depth leads to small changes in tsunami height (Figures 8 to 11), larger intervals of depth variations can be applied in MSZ's tsunami scenarios (for example, depth values of 10, 20, and 30 kilometers). Furthermore, as earthquake depth of 10 and 15 kilometers creates the highest tsunami wave height, in order to reduce the number of scenarios, it is possible to consider one of these two values as the fixed earthquake depth value.

8. References

[1] National Centers for Environmental Information (NCEI) (2017), NGDC/WDS Global Historical Tsunami Database.

[2] Heck, N. H. (1947). List of seismic sea waves. Bulletin of the Seismological Society of America, 37(4), 269-286.

[3] Rashidi, A., Shomali, Z. H., Dutykh, D., & Keshavarz Farajkhah, N. (2020). Tsunami hazard assessment in the Makran subduction zone. Natural Hazards, 100(2), 861-875. https://doi.org/10.1007/s11069-019-03848-1

[4] Rajendran, C. P., Rajendran, K., Shah-Hosseini, M., Beni, A. N., Nautiyal, C. M., & Andrews, R. (2013). The hazard potential of the western segment of the Makran subduction zone, northern Arabian Sea. Natural hazards, 65, 219-239. https://doi.org/10.1007/s11069-012-0355-6

[5] Heidarzadeh, M., Pirooz, M. D., Zaker, N. H., & Yalciner, A. C. (2009). Preliminary estimation of the tsunami hazards associated with the Makran subduction zone at the northwestern Indian Ocean. Natural Hazards, 48, 229-243. https://doi.org/ 10.1007/s11069-008-9259-x

[6] Neetu, S., Suresh, I., Shankar, R., Nagarajan, B., Sharma, R., Shenoi, S. S. C., ... & Sundar, D. (2011). Trapped waves of the 27 November 1945 Makran tsunami: observations and numerical modeling. Natural Hazards, 59, 1609-1618. https://doi.org/10.1007/s11069-011-9854-0

[7] Rastgoftar, E., & Soltanpour, M. (2016). Study and numerical modeling of 1945 Makran tsunami due to a probable submarine landslide. Natural Hazards, 83, 929-945. https://doi.org/10.1007/s11069-016-2356-3

[8] Heidarzadeh, M., & Satake, K. (2017). A combined earthquake–landslide source model for the Tsunami from the 27 November 1945 M w 8.1 Makran earthquake. Bulletin of the Seismological Society of America, 107(2), 1033-1040. ttps://doi.org/10.1785/0120160196

[9] Momeni, P., Goda, K., Heidarzadeh, M., & Qin, J. (2020). Stochastic analysis of tsunami hazard of the 1945 Makran subduction zone Mw 8.1–8.3 earthquakes. Geosciences, 10(11), 452. https://doi.org/10.3390/geosciences10110452

[10] Honarmand, M., Shanehsazzadeh, A., & Zandi, S. M. (2020). 3D numerical simulation of tsunami generation and propagation, case study: Makran tsunami generation and penetrating in Chabahar Bay. Ocean Engineering, 218, 108109. https://doi.org/10.1016/j.oceaneng.2020.108109

[11] Heidarzadeh, M., Pirooz, M. D., & Zaker, N. H. (2009). Modeling the near-field effects of the worst-case tsunami in the Makran subduction zone. Ocean Engineering, 36(5), 368-376. https://doi.org/10.1016/j.oceaneng.2009.01.004

[12] Swapna, M., & Srivastava, K. (2014). Effect of Murray ridge on the tsunami propagation from

Makran subduction zone. Geophysical Journal International, 199(3), 1430-1441.

[13] Akbarpour Jannat, M. R., Rastgoftar, E., & Asano, T. (2017). Tsunami assessment for inundation risk management at chabahar bay facilities in Iran. International Journal of Coastal and Offshore Engineering, 1(2), 27-39. https://doi.org/10.22034/ijcoe.2023.340919.0

[14] Heidarzadeh, M., & Kijko, A. (2011). A probabilistic tsunami hazard assessment for the Makran subduction zone at the northwestern Indian Ocean. Natural hazards, 56, 577-593.

[15] Salah, P., Sasaki, J., & Soltanpour, M. (2021). Comprehensive probabilistic tsunami hazard assessment in the Makran subduction zone. Pure and Applied Geophysics, 1-23. https://doi.org/10.1007/s00024-021-02725-y

[16] Zoljoodi, M., & Zoljoodi, R. (2020). Executive management engineering plans for comparison with tsunami damage. International Journal of Coastal, Offshore and Environmental Engineering, 5(4), 19-23. https://doi.org/10.29252/ijcoe.3.4.19

[17] American Society of Civil Engineers. (2017, June). Minimum design loads and associated criteria for buildings and other structures. American Society of Civil Engineers.

[18] Okada, Y. (1985). Surface deformation due to shear and tensile faults in a half-space. Bulletin of the seismological society of America, 75(4), 1135-1154.

[19] Haberland, C., Mokhtari, M., Babaei, H. A., Ryberg, T., Masoodi, M., Partabian, A., & Lauterjung, J. (2021). Anatomy of a crustal-scale accretionary complex: Insights from deep seismic sounding of the onshore western Makran subduction zone, Iran. Geology, 49(1), 3-7. https://doi.org/10.1130/G47700.1

[20] Noson, L. L., Qamar, A., & Thorsen, G. W. (1988). Washington State Earthquake Hazards. Washington State Department of Natural Resources, Washington Division of Geology and Earth Resources Information Circular 85.

[21] Frohling, E., & Szeliga, W. (2016). GPS constraints on interplate locking within the Makran subduction zone. Geophysical Supplements to the Monthly Notices of the Royal Astronomical Society, 205(1), 67-76. https://doi.org/10.1093/gji/ggw001

[22] Smith, G. L., McNeill, L. C., Wang, K., He, J., & Henstock, T. J. (2013). Thermal structure and megathrust seismogenic potential of the Makran subduction zone. Geophysical Research Letters, 40(8), 1528-1533. https://doi.org/10.1002/grl.50374

[23] Wells, D. L., & Coppersmith, K. J. (1994). New empirical relationships among magnitude, rupture length, rupture width, rupture area, and surface displacement. Bulletin of the seismological Society of America, 84(4), 974-1002.

[24] Byrne, D. E., Sykes, L. R., & Davis, D. M. (1992). Great thrust earthquakes and aseismic slip along the plate boundary of the Makran subduction zone. Journal of Geophysical Research: Solid Earth, 97(B1), 449-478.

[25] Heidarzadeh, M., Pirooz, M. D., Zaker, N. H., & Synolakis, C. E. (2009). Evaluating tsunami hazard in the northwestern Indian Ocean. Tsunami Science Four Years after the 2004 Indian Ocean Tsunami: Part I: Modelling and Hazard Assessment, 2045-2058. https://doi.org/10.1007/s00024-008-0415-8

[26] Rajendran, C. P., Ramanamurthy, M. V., Reddy, N. T., & Rajendran, K. (2008). Hazard implications of the late arrival of the 1945 Makran tsunami. Current Science (00113891), 95(12).

[27] Heidarzadeh, M., Pirooz, M. D., Zaker, N. H., & Mokhtari, M. (2007). Modeling the 1945 Tsunami in the south coast of Iran. the 3rd National Congress of Civil Engineering (in Persian)

[28] Gica, E. (2008). Development of the forecast propagation database for NOAA's Short-term Inundation Forecast for Tsunamis (SIFT).

[29] Schlüter, H. U., Prexl, A., Gaedicke, C., Roeser, H., Reichert, C., Meyer, H., & Von Daniels, C. (2002). The Makran accretionary wedge: sediment thicknesses and ages and the origin of mud volcanoes. Marine Geology, 185(3-4), 219-232. https://doi.org/10.1016/S0025-3227(02)00192-5

[30] Polet, J., & Kanamori, H. (2000). Shallow subduction zone earthquakes and their tsunamigenic potential. Geophysical Journal International, 142(3), 684-702. https://doi.org/10.1046/j.1365-246x.2000.00205.x

[31] Synolakis, C. E., Chen, W. F., & Scawthorn, C. (2003). Tsunami and Seiche in Earthquake Engineering Handbook.

[32] Titov, V. V., & Synolakis, C. E. (1998). Numerical modeling of tidal wave runup. Journal of Waterway, Port, Coastal, and Ocean Engineering, 124(4), 157-171. https://doi.org/10.1061/(ASCE)0733-950X(1998)124:4(157)